1   **Technical Note: Bioaerosol identification by wide particle**

2   **size range single particle mass spectrometry**

3

4   **Xuan Li**[1,2]**, Lei Li**[1,2]**, Zeming Zhuo**[1,2]**, Guohua Zhang**[3]**, Xubing Du**[1,2]**, Xue Li**[1,2]**,**

5   **Zhengxu Huang**[1,2]**, Zhen Zhou**[1,2]**, and Zhi Cheng**[4]

6   [1]Institute of Mass Spectrometry and Atmospheric Environment, Jinan University,

7   Guangzhou, 510632, China

8   [2]Guangdong Provincial Engineering Research Center for On-Line Source

9   Apportionment System of Air Pollution, Guangzhou, 510632, China

10   [3]Guangzhou Institute of Geochemistry, Chinese Academy of Sciences, Guangzhou,

11   510640, China

12   [4]Institute of Systems Engineering, Academy of Military Sciences, Tianjin, 300161,

13   China

14

15   **Correspondence:** Zhi Cheng(chengzh@npec.org.cn)

16

17

18   **Abstract** The sources of bioaerosols are complex and diverse, which have a direct impact on the

19   environment, climate, and human health. The effective identification of bioaerosols in the

20   atmosphere is greatly significant for accurately obtaining the atmospheric chemical characteristics

21   of bioaerosols and making biological early warnings and predictions. To improve the identification

22   ability of bioaerosols, this study detected a variety of bioaerosols and abiotic aerosols based on a

23   single particle aerosol mass spectrometry (SPAMS). Furthermore, the bioaerosol particle

24   identification and classification algorithm based on the ratio of phosphate to organic nitrogen was

25   optimized to distinguish bioaerosols from abiotic aerosols. The results show that 15 kinds of pure

26   fungal aerosols were detected by SPAMS based on a wide range sampling system and that fungal

27   aerosols with a particle size up to 10 μm could be detected. Through the mass spectra peak ratio

28   method of PO_3^-/PO_2^- and CNO^-/CN^-, when discriminating abiotic aerosols, such as disruptive

29   biomass combustion particles, automobile exhaust, and dust, from pure bacterial aerosols, the

30   discrimination degree was up to 97.7%. The optimized ratio detection method of phosphate to

31   organic nitrogen has strong specificity, which can serve as the discriminant basis for identifying

32   bioaerosols in SPAMS source analysis or other analytical processes.

33   **Keywords** Bioaerosol; Single particle aerosol mass spectrometer (SPAMS); Online identification

1   Introduction

34

35   As a crucial component of atmospheric organic aerosols, bioaerosols participate in the

36   weather and climate process as cloud condensation nuclei and ice nuclei (Fröhlich-Nowoisky et al.，

37   2016). Moreover, some aerosols are human allergens, which pose a great threat to human health.

38   At present, the importance of bioaerosols (Burrows et al., 2009) has been fully recognized;

39   however, the sources of bioaerosols are sometimes difficult to identify, given their wide and

40   scattered sources (Li et al., 2021), in addition to the obvious influence of meteorological

41   conditions. This makes the identification of bioaerosols in the environment difficult (Rosch et al.,

42   2006).

43   At present, laser-excited fluorescence spectroscopy is widely employed to detect bioaerosols

44   (Li et al., 2018) due to its strong fluorescence signal, relative ease of operation, long-distance

45   identification of bioaerosols and abiotic aerosols, and determination of single-molecule particle

46   spectra. The fluorescent groups contained in bioaerosol particles are used for their detection in the

47   fluorescence spectrometry method. However, since some inorganic minerals also fluoresce under

48   ultraviolet light excitation, it is difficult to exclude the interference of abiotic fluorescent particles

49   in the identification process. For instance, polycyclic aromatic compounds or humic acids can

50   have similar fluorescence properties (Gabey et al., 2010) and cigarette smoke has similar

51   fluorescence properties to bacteria (Hill et al., 1999). In recent years, the single particle mass

52   spectrometry detection technology of bioaerosols has been developed rapidly, which can obtain

53   the particle size information and chemical composition of single particles in real-time online.

54   However, single particle aerosol mass spectrometry (SPAMS) also has its shortcomings in

55   identifying environmental bioaerosols (Kleefsman et al., 2007). As phosphorus and nitrogen are

56   components of nucleic acids and cell membranes, there is a large number of phosphate ions (PO^-,

57   PO_2^-, and PO_3^-) and organic nitrogen ions (CN^- and CNO^-). Therefore, particles containing

58   phosphate and organic nitrogen in the ambient air (such as biomass combustion products (Wei et

59   al., 2019), fly ash, road dust (Yu et al., 2017), vehicle exhaust (Sodeman et al., 2005), and soil dust

60   (Silva et al., 2000) are often confused with bioaerosols in the detection process. To improve the

61   identification of bioaerosols, Zawadowicz et al. (2017) proposed a classification algorithm of

62   spectral peak ratio based on PO_3^-/PO_2^- and CN^-/CNO^-. When using particle analysis by laser mass

63   spectrometry to discriminate dust and combustion by-products from pollen and bacterial aerosols,

64   the degree of confidence is up to 98%. However, the research on the detection and discrimination

65   of bioaerosols from fungi and other bioaerosols remains insufficient.

66   In addition, the particle size distribution of bioaerosols is generally 0.3–100 μm, while that of

67   viruses is less than 0.3 μm (Smets et al., 2016). The typical particle size of bacteria is 0.25–8 μm,

68   while that of fungi is 1–30 μm, among which the particle size that can cause harm to the human

69 body is generally between 0.4–10 μm. For most of the existing SPAMS, the particle size analysis

70 ability is about 0.1–3 μm, thus the ability of SPAMS to detect fungi, spores, and other large

71 particles is limited. Williams et al. (2013) designed a 7-stage aerodynamic lens (A-lens) to

72 improve the ability of aerodyne aerosol mass spectrometry to detect biological particles. By

73 optimizing the buffer cavity and increasing the sampling pressure of the lens, the transport

74 efficiency of aerosol particles in the size range of 200–5000 nm can reach 100% but that of 10 μm

75 particles is only 22%. At the same time, Cahill et al. (2014) constructed a 7-stage A-lens for the

76 transmission of a single particle in the range of 4–10 μm and found that the transmission

77 efficiency of 10 μm particles was less than 20%, while that of 3 μm particles was close to 0.

78 ATOFMS is attempted to extend to the study of single-cell metabolomics.

79   To improve the ability of SPAMS to detect bioaerosols, a new sampling system (wide particle

80 size range is 0.1–10 μm) was verified in the preliminary design. The particle transport efficiency

81 can reach 100% in the particle size range of 0.15–10 μm. In this study, the advantages of high

82 performance-SPAMS (HP-SPAMS) in the detection of bioaerosols were explored and 10 μm

83 fungal particles were successfully detected. Furthermore, the discrimination method based on the

84 ion ratio of bioaerosol characteristic peak was further optimized and verified, which could

85 successfully discriminate bioaerosols from common disruptors, such as road dust, vehicle exhaust,

86 and biomass combustion products, with a discrimination degree of 97.7%. In addition, this

87 discrimination method had good statistical significance for bacterial aerosols. The analysis of

88 single particle mass spectra is a hard ionization process and laser energy has little effect on the

89 discrimination of this classification method. This method can be used as a discriminant basis for

90 identifying bioaerosols in SPAMS source analysis or other analyses.

91

2 Experiment

2.1 SPAMS

94   The constitution and working principle of SPAMS have been described in detail by Li et al.

95 (2011). In short, SPAMS uses an aerodynamic lens to introduce aerosols from the atmosphere into

96 a vacuum system and focus them into a collimating particle beam. Two successive laser beams are

97 then used to measure the flight speed of particles and calculate their aerodynamic diameter in turn.

98 The high-energy pulsed laser ionizes particles into positive and negative ions at the center of the

99 ion source, which is detected by time-of-flight mass spectrometry.

100   In this study, the performance of HP-SPAMS was improved on the original basis and the

101 resolution of the time-of-flight mass spectrometer was improved using delayed extraction

102 technology (Li et al., 2018). The multi-channel superimposed signal acquisition system improves

103 the sensitivity and dynamic range of instrument detection (Shen et al., 2018). In particular, for the

104 improvement of the sampling system (Zhuo et al., 2021), the whole sampling system consists of

105 five modules: pre-focusing sampling interface, virtual impact concentration device, buffer cavity,

106 7-stage aerodynamic lens, and acceleration nozzle. The pore size was expanded from 0.11 μm to

107 0.22 μm. The numerical results show that the theoretical transport efficiency of particles could

108 reach 100% in the particle size range of 0.15–10 μm, which improved the sampling capacity of

109 SPAMS for coarse particles and provided conditions for the detection of bioaerosols.

110 **2.2 Sample Determination**

111 The 10 strains of bacteria and five strains of fungi determined in this study were standard

112 strains provided by Hexin Kangyuan Medical Technology Co., Ltd. (Guangzhou). The specific

113 names are shown in Table 1. Biological aerosol disruptors often found in the real environment,

114 such as road dust, vehicle exhaust, and biomass combustion products (wheat stalk, corn stalk, and

115 oblate leaf stalk), were selected as the research objects.

116 The preparation steps of the strain sample solution are as follows: 1) Sampling: first, the

117 strains refrigerated at -80℃ were taken out, thawed at room temperature for 1–2 hours, and

118 vortexed using an oscillator to shake the centrifugation tube of the strain sample evenly. 2)

119 Inoculation: on a clean laboratory table, the strain solution adhered to the disposable sterilized

120 inoculating loop, and streak inoculation on the blood agar plate medium was performed. 3)

121 Culture: the streaked culture medium was placed horizontally in a 37℃ constant temperature box

122 for about 24 hours. 4) Sampling: the growth of the samples of 15 strains after the culture is shown

123 in Table 1. The colonies on the surface of the blood agar were slightly scraped with a disposable

124 sterilized inoculating loop, dissolved with 1 mL deionized water in the centrifuge tube, and shaken

125 well. 5) Dilution with water-soluble salt: the bacterial sample aqueous solution was centrifuged for

126 3 min at the rotation speed of 3,000–5,000 rpm. After centrifugation, the sample was precipitated

127 at the bottom of the centrifuge tube and the aqueous solution was absorbed. Then, 1 mL of

128 deionized water was added to dissolve the precipitate, followed by thorough shaking. Step 5 was

129 repeated thrice.

130 The main components of blood agar plate medium used in this experiment were peptone, beef

131 powder, sodium chloride, defiber sheep's blood, agar and deionized water. All media were

132 autoclaved prior to use. Scrape only the upper layer of the culture medium surface to avoid small

133 contaminants of the culture medium itself. Repeated rinsing with deionized water removes excess

134 salt. It should be stressed that no additional fixatives or epoxies were added to the cells before

135 analysis, reducing complications in the interpretation of the mass spectra.

136 The prepared pure bacterial sample solution was mixed with 20 mL of deionized water and

137 atomized using a single nozzle aerosol generator (TSI Inc., Model 9302) to obtain the aerosol

138 particles of the samples. A sheath gas of 80 kPa of clean air was used. The atomized sample
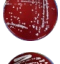
139   aerosol was connected to a silica gel drying tube, whose outlet was connected to the SPAMS inlet

140   and an exhaust port with a high-efficiency particulate air filter. When sampling, 1,000 effectively

141   ionized particle size, and spectrum data were stored in each sample. The experimental flow of

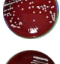142   HP-SPAMS is shown in Fig. 1.

143

144   Table 1 Sample numbers and names of the 15 strains

| number of samples	name	state of bacteria or fungal
#01	Klebsiella pneumoniae	
#02	Salmonella pneumoniae	
#03	Shiga virulent Escherichia coli	
#04	Bordetella bronchitis	
#05	Escherichia coli	
#06	Staphylococcus aureus	
#07	Listeria monocytogenes	
#08	Enterococcus faecium	
#09	Enterobacter cloacae	
#10	Staphylococcus epidermidis	
#11	Candida albicans	
#12	Candida tropicalis	
#13	Candida glabrata	
#14	Aspergillus brasiliensis	
#15	Saccharomyces cerevisiae	

145
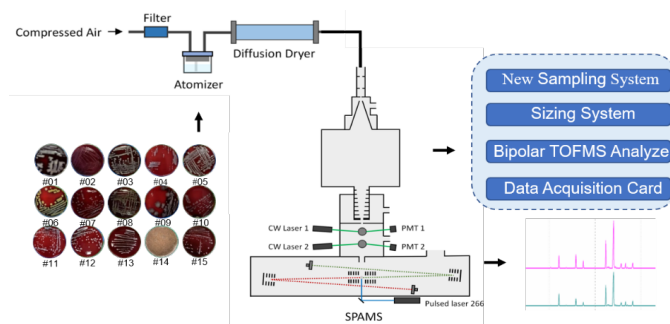
147 Fig. 1 Experimental flow of HP-SPAMS

148 **3 Results and Conclusions**

149 **3.1 Distribution of bioaerosol particle size**

150   The vacuum aerodynamic particle size distribution of the bacterial and fungal particles is

151 shown in Fig. 2. Preliminary experimental results showed that the overall particle size of bacteria

152 was relatively smaller, except for #08 *Enterococcus faecium*. The overall particle size distribution

153 of bacteria was mainly within the range of 0.3–1 μm, thus showing an approximately normal

154 distribution. Jung and Lee (2013) used scanning electron microscopy to observe *Escherichia coli*

155 and *Bacillus subtilis* cells at room temperature, both bacteria with a diameter in the range of 0.5–

156 0.7 μm and a length in the range of 1.1–1.6 μm. Fungi samples (#11, #12, #13, #14, and #15)

157 obtained from pure strain cultures had a much larger proportion of particle size distribution above

158 1 μm than bacteria, and the particle size distribution of three fungi, *Candida albicans*, *Candida*

159 *glabrata*, and *Saccharomyces cerevisiae* were around 0.5–2 μm. Sample #13 *C. glabrata* was

160 concentrated in the range of 1–2.5 μm. Compared with other samples, the samples #11 *C. albicans*

161 and #12 *Candida tropicalis* were similar to the samples #14 *Aspergillus brasiliensis* and #15 *S.*

162 *cerevisiae* in terms of particle size distributions, while the particle size distribution of samples #11

163 and #15 was mainly in the range of 0.25–1.5 μm and the peak was around 0.4 μm. It is worth

164 noting that the particle size of *C. tropicalis* and *A. brasiliensis* were evenly distributed between 0.1

165 μm and 10 μm. Li et al. (2020) used transmission electron microscopy and scanning electron

166 microscopy to investigate primary biological aerosol particles (PBAPs) collected from boreal

167 coniferous forests in the Xiao Hinggan Mountains of China in summer and speculated that the size

168 of rod PBAPs was distributed at 1.4 μm and 3.5 μm and that the two typical peaks were bacterial

169 and fungal particles, respectively.

170   Due to the low transmission efficiency of the aerodynamic lens for large particles and the

171 tendency of large particles to produce inertial impinging wall loss in the process of air transport,

172 especially large particles above 1 μm, the detected particle size distribution was smaller than the

173 real one. Therefore, for the first time, HP-SPAMS was used to measure 10 μm coarse particulate

174 matter under the improvement of the sampling system.
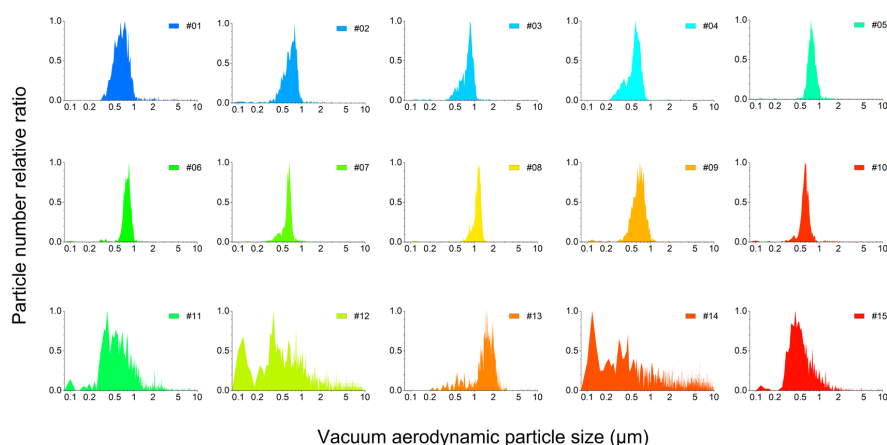
175

176 Fig. 2 Vacuum aerodynamic size distribution of 15 biological samples detected by SPAMS

177 **3.2 Characteristic spectrum of bioaerosols**

178   Zeng et al. (2019) used SPAMS to detect 13 strains of bacteria in 2019 to obtain similar

179 bioaerosol characteristic ions; however, there were fewer characteristic peaks in the negative mass

180 spectrum, and no negative ions with a mass charge ratio greater than 200 were detected, and the

181 overall ionic peak signal was 50–10,000. HP-SPAMS detected the mass spectra of 15 strains of

182 pure bacteria as shown in Fig. 3. Similar to the SPAMS detection results of the same type in the

183 world, they all could effectively measure the phosphate and organic nitrogen ionic peaks of active

184 bacterial aerosols, as well as some amino acid decarboxylic ionic peaks in the positive mass

185 spectrum. Czerwieniec et al. (2005) found similar peaks when detecting vegetative cells of

186 *Bacillus atrophaeus* and speculated that +30, +70, +72, +74, +86, +110, and +120 were

187 decarboxylic ionic peaks of amino acids. The positive ion peaks were mainly ^{30}[Glycine-COOH]$^+$,

188 ^{70} [Proline-COOH]$^+$, ^{72} [Valine-COOH]$^+$, ^{74} [Threonine-COOH]$^+$, ^{86} [Leucine-COOH]$^+$,

189 ^{110} [Histidine-COOH]$^+$, and ^{120} [Phenylalanine-COOH]$^+$. Srivastava et al. (2005) speculated that

190 +59, +81, +84, and +88 ionic peaks were organic fragments containing nitrogen, among which

191 ^{84} [C_5NH_{10}]$^+$ with a strong signal was also found in the detection of this study. The negative ionic

192 peaks were mainly organic nitrogen $^{26}CN^-$, $^{42}CNO^-$, phosphate $^{63}PO_2^-$, $^{79}PO_3^-$, $^{97}H_2PO_4^-$,

193 $^{159}H(PO_3)_2^-$, $^{199}NaH_2P_2O_7^-$, and other common biological ionic peaks.

194   More abundant ion characteristics were obtained by HP-SPAMS. On the original basis, the

195 decarboxylic ionic peaks of serine and alanine ^{44} [Alanine-COOH]$^+$ and ^{60} [Serine-COOH]$^+$ were

196 supplemented and the signal intensity in the HP-SPAMS detection results was relatively strong.

197 The negative ion peaks $^{261}NaH(PO_3)_3^-$ and $^{277}NaH(PO_3)_2(PO_4)^-$ with a mass charge ratio greater

198 than 250 were speculated and added. Exponential pulse delayed extraction technology（Chen et al.，

199 2020) not only solves the hit rate and resolution problems of SPMS but also improves the ion

200 signal intensity by multiple times, thereby providing conditions for obtaining the complete mass

201 spectrum characteristics of bioaerosols. More characteristic peaks can make it easier to distinguish

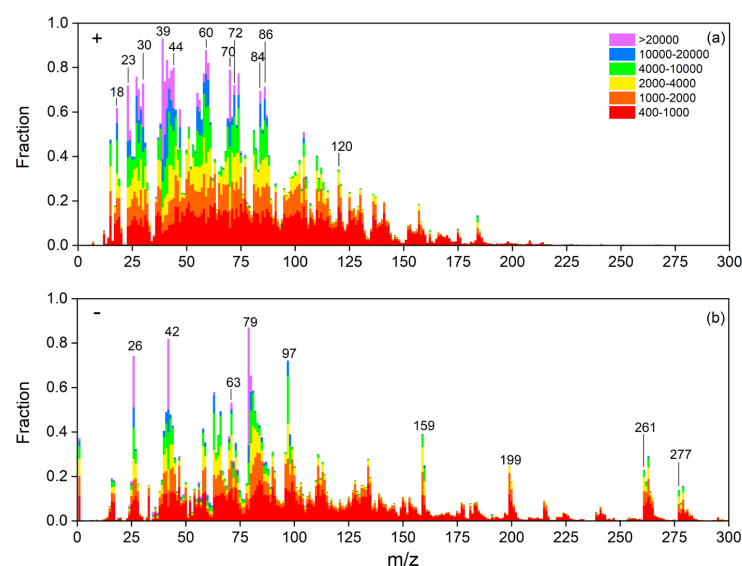202 whether or not a single particle is a bioaerosol.

203

204 Fig. 3 Stacking diagram of the area of all bioaerosol ion peaks; (a) Positive mass spectrum; (b) Negative mass

205 spectrum

3.3 Bioaerosol identification based on characteristic peak ratio

207   HP-SPAMS can accurately screen out bioaerosols according to their characteristic ions.

208 However, due to the different intensity of ion signals in the single-particle spectrum, when the

209 signal of the characteristic peak is weak, the spectrum will be ignored and the bioaerosols cannot

210 be completely extracted. Zawadowicz proposed that $^{26}CN^-$, $^{42}CNO^-$, $^{63}PO_2^-$, and $^{79}PO_3^-$ could be

211 used as characteristic peaks of bioaerosol discrimination to distinguish bioaerosols from abiotic

212 aerosols in a larger proportion. In the actual environment, many inorganic particles contain

213 bioaerosol characteristic ion phosphate and organic nitrogen peaks. Organic nitrogen and

214 phosphate ionic peaks with strong signals also appear in biomass combustion products, vehicle

215 exhaust, and road dust measured by HP-SPAMS, as shown in Fig. 4. Therefore, when using

216 phosphate and organic nitrogen ionic peaks alone to identify bioaerosols in the environment, at

217 least 89% of vehicle exhaust, 49.5% of dust, and 58.3% of biomass combustion products have

218 interference, which cannot be directly used as a sufficient condition to distinguish bioaerosols.
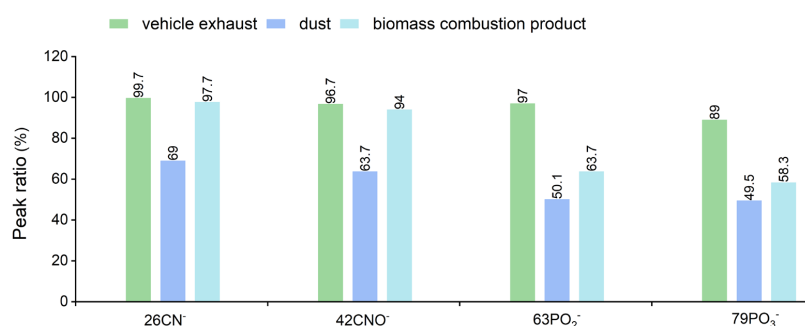
Fig. 4 Comparison of the frequency of four ion peaks in abiotic aerosols

Data classification based on HP-SPAMS, which is the peak height ratio of the mass spectra peak of PO_3^-/PO_2^- and CNO^-/CN^-, was used to distinguish bioaerosols from their disruptors. The scatter distribution of PO_3^-/PO_2^- and CNO^-/CN^- was obtained by capturing the corresponding ionic peak height. As shown in Fig. 5, the distribution of bioaerosols was significantly different from that of biomass combustion products, vehicle exhaust, and dust. In particular, the scatter distribution positions of PO_3^-/PO_2^- and CNO^-/CN^- were significantly different from that of vehicle exhaust. Moreover, it was concentrated in a certain range of values. Bioaerosols were classified as one class, while aerosols produced by vehicle exhaust, dust, and biomass combustion products were classified as another class. The proportion interval of the bioaerosols PO_3^-/PO_2^- and CNO^-/CN^- measured by SPAMS were concentrated at (3,200) and (0.7, 7), respectively, while those of abiotic aerosols were at (0.2, 3) and (0.02, 2), respectively. Furthermore, using the support vector machine (SVM), a supervised machine learning algorithm, the discrimination degree between bioaerosols and abiotic aerosols was up to 97.7%. This indicates that HP-SPAMS had a strong detection specificity on the phosphate and organic nitrogen ratio between bioaerosols and abiotic aerosols. It is possible to use it as the discriminant basis for identifying bioaerosols in the SPAMS source analysis or other analyses. Compared with the traditional single discrimination method via life characteristic elements, such as nitrogen and phosphorus, this method has a higher discrimination degree.
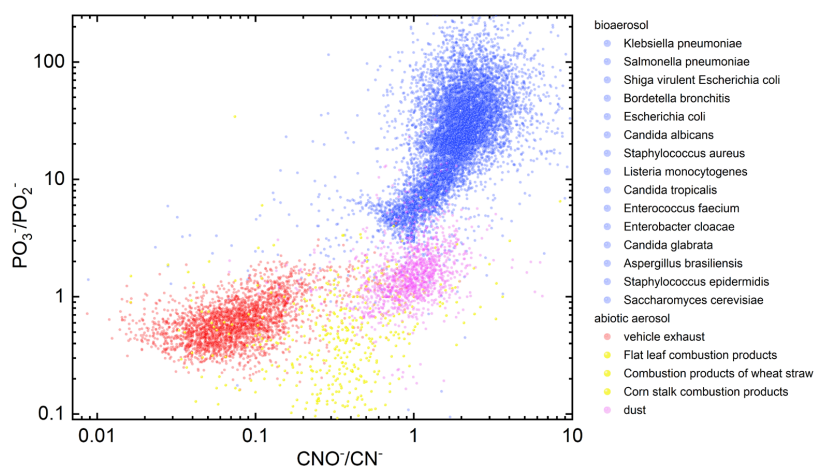
9 / 16

239

Fig. 5 Scatterplot of the bioaerosol and abiotic aerosol CNO^-/CN^- and PO_3^-/PO_2^-

241   The premise of this classification method is that there are four characteristic peaks. However,
242   the actual research showed that when the threshold of the effective peak was set high, part of the
243   weak signal peaks would be filtered out; however, when the threshold was set low, there was noise
244   interference in the collected signals. Through a series of equivalent gradient threshold settings, the
245   effective peak threshold of 10 mV was determined. The average frequency of the characteristic
246   peaks in the bacterial aerosols was generally higher than that of the fungal aerosols, as shown in
247   Table 2. At least, 82.9% of bacterial aerosols and 52.8% of fungal aerosols could be effectively
248   discriminated against. The discrimination method based on the characteristic peak ratio had a high
249   identification rate for bacterial aerosols. Fungi and bacteria have great differences in terms of
250   morphology and structure. Bacteria are mainly coccus, bacillus, and spiral, while fungi are mainly
251   subcellular and multicellular. In addition, fungi have nuclei. In the detection process, bacterial
252   aerosols are more easily ionized to produce effective mass spectra peaks.

253   Table 2 The average frequency of the characteristic ionic peak of bioaerosol

Species	CN^-	CNO^-	PO_2^-	PO_3^-
Bacteria	92.9%	96.5%	82.9%	97.6%
Fungus	63.8%	70.4%	52.8%	75.3%

254   ### 3.4 Influence analysis of laser energy

255   SPAMS single-step laser desorption is a difficult ionization process in which organic
256   compounds produce ion fragments of different degrees. Noble et al. (1996) proposed that in single
257   particle mass spectrometry analysis, it is difficult to determine the morphology of organic
258   compounds due to the extensive fragmentation caused by the ionization process. Cornwell et al.

259 (2022) proposed that the ion signals of dust and biological particles were very sensitive to

260 ionization conditions and that total positive ion intensity was used to characterize the mass

261 spectral relationship between different dust and biological particles. Through this method,

262 environmental particles with both dust and characteristic biological spectra fingerprints were

263 successfully excluded from the classification of biological particles. Liu et al. (2021) used *Bacillus*

264 *thuringiensis* to explore the influence of different laser pulse energies on SPAMS and found that

265 particles did not ionize when the laser energy was lower than 0.2 mJ and that the ionic peak

266 increased significantly when the laser energy was higher than 1.5 mJ; they also found that the

267 ionic peak integrity was the best when the laser energy was about 0.5 mJ. Too high or too low

268 energy was not conducive to the discovery of the characteristic mass spectrum. To verify the

269 influence of ionized laser energy on this analysis method, different laser energies of 0.5, 0.75, 1.0,

270 1.25, and 1.5 mJ were selected and *Staphylococcus aureus* was taken as an example to explore the

271 influence of ionized laser energy on the ionic peak ratio. As shown in Fig. 6, as the energy

272 increased, the ionization degree increased with more fragmented ions, the ratio of PO_3^-/PO_2^- and

273 CNO^-/CN^- decreased, and more PO_3^- and CNO^- were ionized as PO_2^- and CN^-, respectively.
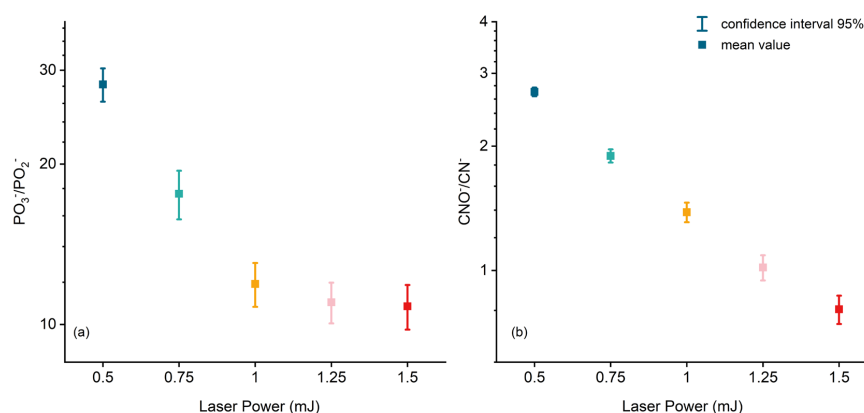

Fig. 6 Distribution of PO_3^-/PO_2^- (a) and CNO^-/CN^-(b)

276 Furthermore, the discrimination degree of ionized laser energy on bioaerosols under different

277 ratios was compared. The biological aerosol (*S. aureus*) and abiotic aerosol (dust) were selected

278 under the laser energy of 0.5 mJ. Using SPAMS, it was found that the ratio interval of PO_3^-/PO_2^-

279 and CNO^-/CN^- was concentrated in (5, 70) and (0.8, 3), while that of dust aerosol was (0.7, 3) and

280 (0.5, 2), respectively. When the laser energy was 1.5 mJ, the ratio interval of bioaerosols was (2,

281 30) and (0.7, 3), while that of dust aerosols was (0.6, 3) and (0.6, 2). As shown in Fig. 7, The

282 interval of biological aerosols was gradually changing and the trends of horizontal and vertical

283 coordinates were both decreasing, while the scatter interval of abiotic aerosols was almost

284 unchanged. According to the SVM algorithm, the discrimination degree of bacterial aerosols and

285 dust under 0.5, 0.75, 1.0, 1.25, and 1.5 mJ energies were 96.6%, 97.4%, 97.1%, 96.5%, and 97.8%,

286 respectively, indicating that the ionized laser had little effects on discriminating biological aerosols

287 and dust disruptors.
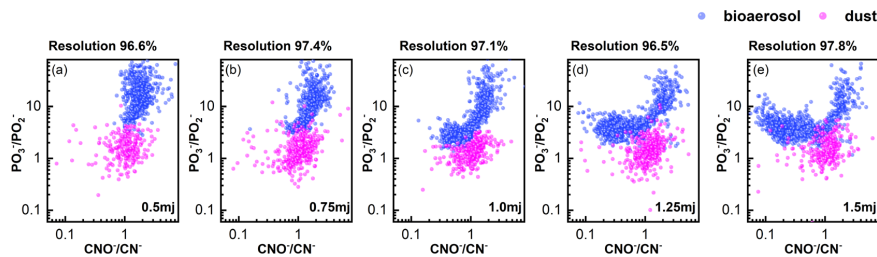
289 Fig. 7 Scatter distribution of the bioaerosol and dust aerosol CNO^-/CN^- and PO_3^-/PO_2^-

290 Under the condition of a constant effective peak threshold, the frequency of phosphate and

291 organic nitrogen ionic peaks of bacterial aerosol and dust changed with the change of the ionized

292 laser energy, as shown in Fig. 8. When the laser energy was 0.5 mJ, the peak output rate of both

293 bioaerosol and dust was the lowest and the influence on abiotic aerosols was larger, with a peak

294 output rate of 34%. When using this classification method for discrimination, it is only necessary

295 to discriminate against 28.7% of dust particles. When the laser energy was 1.5 mJ, the peak output

296 of four *S. aureus* ionic peaks was the highest, while that of the dust was the lowest. At this time,

297 the highest proportion of bacterial aerosols (94.6%) and the lowest proportion of dust particles

298 (31.1%) could be statistically discriminated against. Under the same laser energy, the overall peak

299 output of abiotic aerosols was about 40% lower than that of biological aerosols. Different types of

300 particles had different laser energy requirements. In addition, the variation trend of CNO^- and PO_3^-

301 was the same as that of CN^- and PO_2^-, respectively; however, the phosphate ionic peaks (PO_3^- and

302 PO_2^-) were more affected by the laser energy. In conclusion, when the ionized laser energy was 1.5

303 mJ, the classification method of the ionic peak ratio was more effective in discriminating
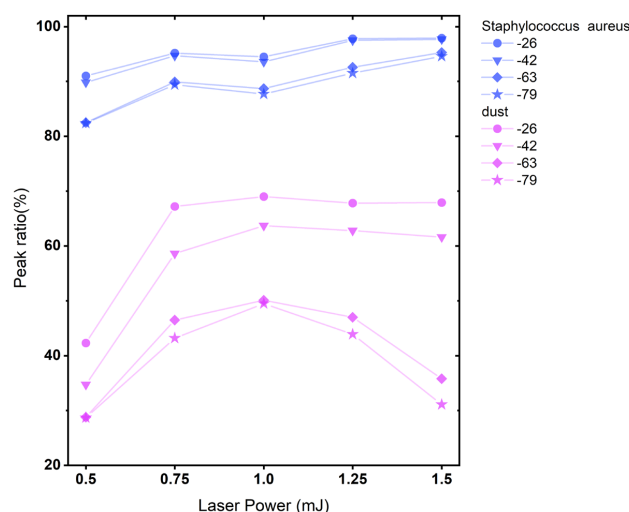
304 bioaerosols.

Fig. 8 Peak rate diagram of the characteristic peak output under different laser energies

4 Conclusions

The performance of SPAMS and the improvement of the sampling system have improved the ability to identify bioaerosols. HP-SPAMS was used for the first time to detect fungal particles with a particle size of 10 μm, which provided a good technical basis for the detection of biological aerosols with large particle sizes in the environment. With the improvement of the instrument performance, the single-particle spectrum of bioaerosol showed decarboxylic ionic peaks of serine and alanine ^{44}[Alanine-COOH]$^+$ and ^{60}[Serine-COOH]$^+$ and phosphate ionic peaks ^{261}NaH(PO$_3$)$_3^-$ and ^{277}NaH(PO$_3$)$_2$(PO$_4$)$^-$. A more unique fingerprint spectrum than the original study was obtained. The bioaerosol identification method based on the characteristic peak ratios PO$_3^-$/PO$_2^-$ and CNO$^-$/CN$^-$ can effectively discriminate bioaerosol from three kinds of commonly seen abiotic disruptors, with the discrimination degree up to 97.7%. In addition, due to the influence of laser ionization efficiency, the effective mass spectra peak ratio of bacterial aerosol generation is higher, thus it is more suitable for this method. The ionized laser energy has a certain influence on the integrity of the ionic peak but hardly affects the identification accuracy of bioaerosols. This study showed that the SPAMS detection technology of bioaerosols has the potential to be a new method for real-time online identification of bioaerosols.

Data availability. These data can be publicly accessible in free.

Author contributions. LL and ZC designed the study; XL and ZMZ performed the experiments; GHZ, XBD, XL, ZXH and ZZ participated in data analysis and result discussion; XL and LL

328   wrote the paper with the input from all authors.

329

330   Competing interests. The authors declare that they have no conflict of interest.

331

337

338

339   References

340

341   Burrows, S. M., Elbert, W., Lawrence, M. G., and Poschl, U.: Bacteria in the global atmosphere – Part
342   1: Review and synthesis of literature data for different ecosystems, Atmos. Chem. Phys.,
343   9 ,10777-10827, https://doi.org/10.5194/acp-9-9263-2009, 2009.

344   Cahill, J. F., Darlington, T. K., Wang, X., Mayer, J., Spencer, M. T., Holecek, J. C., Reed, B. E. and
345   Prather, K. A.: Development of a High-Pressure Aerodynamic Lens for Focusing Large Particles (4–
346   10 μm) into the Aerosol Time-of-Flight Mass Spectrometer, Aerosol Sci. Technol., 48 , 948-956,
347   https://doi.org/10.1080/02786826.2014.947400, 2014.

348   Chen, Y., Kozlovskiy, V., Du, X., Lv, J., Nikiforov, S., Yu, J., Kolosov, A., Gao, W., Zhou, Z., Huang, Z.
349   and Li, L., Increase of the particle hit rate in a laser single-particle mass spectrometer by pulse
350   delayed   extraction   technology,   Atmos.   Meas.   Tech.,   13,   941-949,
351   https://doi.org/10.5194/amt-13-941-2020, 2020.

352   Cornwell, G. C., Sultana, C. M., Petters, M. D., Al-Mashat, H., Rothfuss, N. E., Mohler, O., Demott, P.
353   J., Martin, A. C., and Prather, K. A.: Discrimination between individual dust and bioparticles using
354   aerosol   time-of-flight   mass   spectrometry,   Aerosol   Sci.   Technol.,
355   https://doi.org/10.1080/02786826.2022.2055994, 2022.

356   Czerwieniec, G. A., Russell, S. C., Lebrilla, C. B., Coffee, K. R., Riot, V., Steele, P. T., Frank, M., and
357   Gard, E. E.: Improved sensitivity and mass range in time-of-flight bioaerosol mass spectrometry
358   using   an   electrostatic   ion   guide,   J.   Am.   Soc.   Mass   Spectrom.,   16 ,   1866-1875,
359   https://doi.org/10.1016/j.jasms.2005.06.013, 2005.

360   Fröhlich-Nowoisky, J., Kampf, C. J., Weber, B., Huffman, J. A., Pöhlker, C., Andreae, M. O.,
361   Lang-Yona, N., Burrows, S. M., Gunthe, S. S., Elbert, W., Su, H., Hoor, P., Thines, E., Hoffmann, T.,
362   Després, V. R., and Pöschl, U.: Bioaerosols in the Earth system: Climate, health, and ecosystem
363   interactions, Atmos. Res., 182 , 346-376, https://doi.org/10.1016/j.atmosres.2016.07.018, 2016.

364   Gabey, A. M., Gallagher, M. W., Whitehead, J., Dorsey, J. R., Kaye P. H., and Stanley W. R.:
365   Measurements and comparison of primary biological aerosol above and below a tropical forest
366   canopy using a dual channel fluorescence spectrometer, Atmos. Chem. Phys., 10 , 4453-4466,
367   https://doi.org/10.5194/acp-10-4453-2010, 2010.

368   Hill, S. C., Pinnick, R. G., Niles, S., Pan, Y. L., Holler, S., Chang, R. K., Bottiger, J., Chen, B. T., Orr C.

369   S., and Feather, G.: Real-time measurement of fluorescence spectra from single airborne biological

370   particles,FieldAnal.Chem.Technol.,3,

371   https://doi.org/10.1002/(SICI)1520-6521(1999)3:4/53.0.CO;2-7, 1999.

372   Jung, J. H. and Lee, J. E.: In situ real-time measurement of physical characteristics of airborne bacterial

373   particles, Atmos. Enviro., 81, 609-615, https://doi.org/10.1016/j.atmosenv.2013.09.018, 2013.

374   Kleefsman, I., Stowers, M. A., Verheijen, P. J. T., Wuijckhuijse, A. L. van, Kientz, C. E., and

375   Marijnissen, J. C. M.: Bioaerosol analysis by single particle mass spectrometry, Part. Part. Syst.

376   Charact., 24 ,85-90, https://doi.org/10.1002/ppsc.200601049, 2007.

377   Li, L., Liu, L., Xu, L., Li, M., Li, X., Gao, W., Huang, Z., and Cheng, P.: Improvement in the Mass

378   Resolution of Single Particle Mass Spectrometry Using Delayed Ion Extraction, Int. J. Mass

379   Spectrom., 29 ,2105-2109, https://doi.org/10.1007/s13361-018-2037-4, 2018.

380   Li, L., Huang, Z., Dong, J., Li, M., Gao, W., Nian, H., Fu, Z., Zhang, G., Bi, X., Cheng, P., and Zhou,

381   Z.: Real time bipolar time-of-flight mass spectrometer for analyzing single aerosol particles, Int. J.

382   Mass Spectrom., 303 , 118-124, https://doi.org/10.1016/j.ijms.2011.01.017, 2011.

383   Li, X., Ran, B., Wu, W., Wang, Q., Tong, Z., Zhang, X., and Li, Y.: Progress in the application of

384   fluorescence spectroscopy in biological aerosol monitoring, Mil. Med., 42 , 464-470,

385   https://doi.org/10.7644/j.issn.1674-9960.2018.06.015, 2018.

386   Li, W., Liu, L., Xu, L., Zhang, J., Yuan, Q., Ding, X., Hu, W., Fu, P., and Zhang, D.: Overview of

387   primary biological aerosol particles from a Chinese boreal forest: Insight into morphology, size, and

388   mixing   state   at   microscopic   scale,   Sci.   Total   Environ.,   719   ,   137520-137533,

389   https://doi.org/10.1016/j.scitotenv.2020.137520, 2020.

390   Li, Y., Ma, T., Du, S., Xie, W., Zhang, H., and Xie, Z.: Review on source emission and source

391   identification of bioaerosols in the atmosphere, J. Earth Sci. Environ., 43 , 315-331,

392   https://doi.org/10.19814/j.jese.2020.11018, 2021.

393   Liu, C., Li, B., Liu, C., Li, M., and Zhou, Z.: Analysis of single-cell microbial mass spectra profiles

394   from single-particle aerosol mass spectrometry, Rapid Commun. Mass Spectrom., 35 , 9069-9078,

395   https://doi.org/10.1002/rcm.9069, 2021.

396   Noble, C. A., and Prather, K. A.: Real-Time Measurement of Correlated Size and Composition Profiles

397   of Individual Atmospheric Aerosol Particles, Environ. Sci. Technol., 30 , 2667-2680,

398   https://doi.org/10.1021/es950669j, 1996.

399   Rosch, P., Harz, M., Peschke, K. D., Ronneberger, O., Burkhardt, H., Schule, A., Schmauz, G., Lankers,

400   M., Hofer, S., Thiele, H., Motzkus, H. W., and Popp, J.: On-line monitoring and identification of

401   bioaerosols, Anal. Chem., 78 , 2163-2170, https://doi.org/10.1021/ac0514974, 2006.

402   Shen, W., Dai, X., Huang, Z., Hou, Z., Cai, W., Du, X., Zhou, Z., Li, M., and Li, L.: Improvement of

403   the Dynamic Range of Data Acquisition System in Single particle mass spectrometry, J. Chinese

404   Cinemas., 39 ,331-336, https://doi.org/10.7538/zpxb.2017.0119, 2018.

405   Silva, P. J., Carlin, R. A., and Prather, K. A.: Single particle analysis of suspended soil dust from

406   Southern California, 34，1811-1820. https://doi.org/10.1016/S1352-2310(99)00338-6, 2000.

407   Smets, W., Moretti, S., Denys, S., and Lebeer, S.: Airborne bacteria in the atmosphere: Presence,

408   purpose,   and   potential,   Atmos.   Environ.,   139,214-221,

409   https://doi.org/10.1016/j.atmosenv.2016.05.038, 2016.

410   Sodeman, D. A., Toner, S. M., and Prather, K. A.: Determination of single particle mass spectral

411   signatures   from   light-duty   vehicle   emissions,   Environ.   Sci.   Tech.,   39   ,   4569-4580,

412   https://doi.org/10.1021/es0489947, 2005.

413 Srivastava, A., Pitesky, M. E., Steele, P. T., Tobias, H. J., Fergenson, D. P., Horn, J. M., Russell, S. C.,
414   Czerwieniec, G. A., Lebrilla, C. B., Gard, E. E., and Frank, M.: Comprehensive Assignment of Mass
415   Spectral Signatures from Individual Bacillus atrophaeus Spores in Matrix-Free Laser
416   Desorption/Ionization Bioaerosol Mass Spectrometry, Anal. Chem., 77 ,3315-3323,
417   https://doi.org/10.1021/ac048298p, 2005.
418 Wei, M., Xu, C., Xu, X., Zhu, C., Li, J., and Lv, G.: Size distribution of bioaerosols from biomass
419   burning emissions: Characteristics of bacterial and fungal communities in submicron (PM1.0) and
420   fine (PM2.5) particles, Ecotoxicol. Environ. Saf., 171 , 37-46,
421   https://doi.org/10.1016/j.ecoenv.2018.12.026, 2019.
422 Williams, L. R., Gonzalez, L. A., Peck, J., Trimborn, D., McInnis, J., Farrar, M. R., Moore, K. D.,
423   Jayne, J. T., Robinson, W. A., Lewis, D. K., Onasch, T. B., Canagaratna, M. R., Trimborn, A., Timko,
424   M. T., Magoon, G., Deng, R., Tang, D., Blanco, E. d. l. R., Prévôt, A. S. H., Smith, K. A., and
425   Worsnop, D. R.: Characterization of an aerodynamic lens for transmitting particles greater than 1
426   micrometer in diameter into the Aerodyne aerosol mass spectrometer, Atmos. Meas. Tech., 6 ,
427   5033-5063, https://doi.org/10.5194/amtd-6-5033-2013, 2013.
428 Yu, N., Huang, B., Li, M., Cheng, P., Li, L., Huang, Z., Gao, W., and Zhou, Z.: Single particle mass
429   spectrometry characteristics of atmospheric fine particulate dust sources, China Environ. Sci.,
430   37 ,1262-1268, https://doi.org/10.3969/j.issn.1000-6923.2017.04.008, 2017.
431 Zawadowicz, M. A., Froyd, K. D., Murphy, D. M., and Cziczo, D. J.: Improved identification of
432   primary biological aerosol particles using single-particle mass spectrometry, Atmos. Chem. Phys.,
433   17 ,7193-7212, https://doi.org/10.5194/acp-17-7193-2017, 2017.
434 Zeng, Z., Yu, J., Liu, P., Huang, F., Chen, Y., Huang, Z., Gao, W., Li, M., Zhou, Z., and Li, L.: Analysis
435   of bacterial aerosol particles by single particle aerosol mass spectrometer, Anal. Chem., 47 ,
436   1344-1351, https://doi.org/10.19756/j.issn.0253-3820.191202, 2019.
437 Zhuo, Z., Su, B., Xie, Q., Li, L., Huang, Z., Zhou, Z., Mai, Z., and Tan G.: Simulation design and
438   experimental study of aerodynamics particle concentrator for single particle mass spectrometry, J.
439   Vac. Sci. Technol., 41 , 441-447, https://doi.org/10.13922/j.cnki.cjvst.202008026, 2021.
440
441